Self-powered supercapacitive microbial fuel cell: The ultimate way of boosting and harvesting power

Self-Powered Supercapacitive Microbial Fuel Cell: The Ultimate Way of Boosting and Harvesting Power

Carlo Santoro[a,†], *Francesca Soavi[b,†], Alexey Serov[a], Catia Arbizzani[b], **Plamen Atanassov[a]

[a] Department of Chemical & Biological Engineering, Center for Micro-Engineered Materials (CMEM), University of New Mexico, Albuquerque, NM 87131, USA.

[b] Department of Chemistry "Giacomo Ciamician", Alma Mater Studiorum - Università di Bologna, Via Selmi, 2, 40126 Bologna, Italy.

Corresponding authors:

* Francesca Soavi, Department of Chemistry Giacomo Ciamician, Alma Mater Studiorum- Università di Bologna, Via Selmi, 2, Bologna, Italy, e-mail: francesca.soavi@unibo.it

** Plamen Atanassov, Department of Chemical & Biological Engineering, Center for Micro-Engineered Materials (CMEM), University of New Mexico, Albuquerque, NM 87131, USA, e-mail: plamen@unm.edu

† The two authors have contributed equally to the manuscript

Abstract

In this work, for the first time, we demonstrate a supercapacitive microbial fuel cell which integrates the energy harvesting function of a microbial fuel cell (MFC) with the high power operation of an internal supercapacitor. The pursued strategies are: i) the increase of the cell voltage by the use of high potential cathodes like bilirubin oxidase (BOx) or iron-aminoantipyrine (Fe-AAPyr); ii) the use of an additional capacitive electrode (additional cathode, AdC) which is short-circuited with the MFC cathode and coupled with the MFC anode (MFC-AdC). The high working potential of BOx cathode and the low impedances of the additional capacitive electrode and the MFC anode permitted to achieve up to 19 mW (84.4 Wm^{-2}, 152 Wm^{-3}), the highest power value ever reported for MFCs. Exploiting the supercapacitive properties of the MFC electrodes allows the system to be simpler, cheaper and more efficient without additional electronics management added with respect to an MFC/external supercapacitor coupling. The use of the AdC makes it possible to decouple energy and power and to achieve recharge times in the order of few seconds making the system appealing for practical applications.

Keywords: microbial fuel cell, supercapacitor, additional cathode, EDLC, high current/power

1. Introduction

Microbial fuel cell (MFC) is a promising biotechnology for multiple applications such as wastewater treatment and energy production from organic compounds (Rinaldi et al., 2008). Enhancement of MFCs performance through anode and cathode electrodes materials development has been the main focus of the past decade for the scientists all over the world (Rinaldi et al., 2008). In general, MFCs can be based on anodes made of carbonaceous (Wei et al., 2011) and not carbonaceous electro-conductive materials (Pocaznoi et al., 2012; Guerrini et al., 2014). Anodes feature high surface area in order to accommodate electroactive bacteria that degrade organics and transfer electrons through an external load. On the other side, cathode catalysts can be from different families of: i) carbonaceous high surface materials (Watson et al. 2013), ii) platinum-based materials (Liu et al., 2015), iii) non-platinum based materials (Antolini, 2015), iv) enzymatic (Schaetzle et al., 2009; Higgins et al. 2011), and v) microbial (Jang et al., 2013; Ishii et al. 2014). Such organic/inorganic materials as well as biotic matter work as catalysts or co-catalyst enhancing the oxygen reduction rate and complete the redox reaction of the MFC. It has been previously shown that at neutral working pH, enzymes (bilirubin oxidase and laccase) based catalysis posses the highest open circuit potentials (OCPs) among the existing catalysts for oxygen reduction reaction (ORR) (Mano et al., 2003; Soukharev et al., 2004).

Current/power generated from MFC systems is over 3 orders of magnitude lower compared to traditional hydrogen- or methanol-fuelled FC (Logan and Rabaey, 2012) and therefore a smart design is necessary in order to harvest the low energy produced and for

66 the subsequent delivering of the high power pulses which are required for powering
67 devices. Supercapacitors are electrochemical energy storage systems which deliver high
68 specific power (up to 10 kW kg^{-1}) at required energy levels (Conway, 1999).
69 Electrochemical double layer capacitors (EDLC) use high surface area carbon electrodes
70 that store/deliver charge by an intrinsically fast and highly reversible electrostatic process
71 (Béguin et al., 2014).
72 Supercapacitors have been externally combined to the MFCs in order to harvest
73 appropriately the energy of the system. The external supercapacitors are recharged by the
74 MFCs and provide high power output during the discharge. This combination has been
75 already investigated by several groups (Wang et al.; 2015). The smart design and
76 efficient series/parallel connection of MFCs with external supercapacitors allowed to
77 power small electronics devices (Papaharalabos et al., 2013, 2014), sensors (Donovan et
78 al., 2011, 2013; Di Lorenzo et al., 2014; Ewing et al., 2014; Dewan et al., 2014; Park et
79 al. 2012), a mobile phone (Ieropoulos et al., 2013), robotics prototypes (Ieropoulos et al.,
80 2005, 2010, 2012) and the pump required to manage the wastewater flow in MFCs
81 (Ledezma et al., 2013).
82 The size of the supercapacitor to be connected with the MFC is a crucial design point.
83 Indeed, the commercially available EDLCs with capacitance on the order of Farads
84 require a substantial recharging time (on the order of several min or even hours) at the
85 low current regimes of MFCs (on the orders of μA). Every generated high current/power
86 pulse requires a long time before its repetition, and consequently the tool that is powered
87 by the MFC/external EDLC is switched on periodically, with long standby steps.

88 The capacitive behavior of the MFC anode has been recently investigated (Deeke et al.,
89 2012; Feng et al., 2012). It has been also reported an MFC anode decoration with
90 ruthenium oxide to improve the capacitive response of MFCs (Lv et al., 2012) but its
91 high cost prevents the usage in large scale MFCs.
92 Designing and improving the capacitive response of the MFC electrodes is a challenging
93 task for creating an integrated MFC-internal supercapacitor system. The capacitive
94 electrodes are expected to accomplish high power discharges, being simultaneously
95 recharged by the MFC redox reactions taking place at the electrode/organics containing
96 solution and electrode/O_2 interfaces.
97 This approach has been already exploited in the field of biofuel cells where the first use
98 of enzymatic biofuel cells (BFC) as internal supercapacitor was recently demonstrated by
99 Pankratov et al. (2014a; 2014b). In this case, the high surface area, carbonaceous anode
100 and cathode of the BFC operated as the electrodes of the supercapacitor. Higher
101 performances have been recently obtained by Agnès et al. (2014) using a glucose-oxygen
102 enzymatic biofuel cell with maximum open circuit voltage of ≈800 mV. The BFC-
103 supercapacitor hybrid system had the highest power achieved of approximately 18 mW
104 (Agnès et al., 2014).
105 To our best knowledge, for the first time, in this study we report on supercapacitive
106 MFCs where anode and cathode simultaneously harvest energy from wastewater and
107 work as self-powered EDLC. The power delivered by supercapacitors increases with cell
108 voltage and with the decrease of the equivalent series resistance (ESR). We demonstrate
109 how the power output of the MFC can be dramatically improved by two strategies: i) the
110 use of non-platinum group metal, like iron-aminoantipyrine (Fe-AAPyr) and of bilirubin

oxidase (BOx) cathodes to increase cell voltage, and ii) the usage of a third, capacitive electrode based on high surface area carbon to decrease ESR. The latter is an "additional cathode" (AdC) which is short-circuited with the MFC cathode and is coupled with the MFC anode to give a self-powered supercapacitor (MFC-AdC). This is the first time that the concept of AdC electrode is used. The proof-of-concept is demonstrated using a commercial high surface area carbon brush as the additional cathode and by galvanostatic tests at different currents from 1mA up to 45 mA.

2. Materials and Methods

2.1 MFC configuration and electrolyte composition

Single glass bottle MFC (Cataldo Arbore, Milan, Italy) with 125 mL volume was used. A lateral hole of 2.25 cm^2 allowed the insertion of the cathode that was there screwed using a metallic clamp. Membraneless configuration allowed the exposure of anode and cathode to the same electrolyte. A reference electrode (Ag/AgCl 3M KCl) was included for the basic electrochemical studies.

The electrolyte was composed of a mixture of 50% volume of activated sludge from Albuquerque Southeast Water Reclamation Facility (New Mexico, USA) and 50% volume of phosphate buffer saline solution (PBS) and KCl 0.1M. PBS was made using KH_2PO_4 (1.77 g) and K_2HPO_4 (15.16 g). The pH of the electrolyte was 7.5±0.02. An air breathing cathode configuration was used and the tests were run in ambient conditions. The experiments have been carried out in Albuquerque at a constant temperature that was

22±1 °C and at 1600 meters above sea level. At that altitude, oxygen concentration is roughly 20% lower compared to sea level due to the lower air pressure. This parameter has to be taken into account when comparing the performance of air-breathing MFCs.

2.2 MFC electrode materials and additional cathode material

Anode electrodes were based on a carbon brush (Millirose, USA) of diameter 3 cm, length of 3 cm and projected area of 9 cm^2. The anodes were pre-colonized by mixed cultures bacteria taken from previous experiments running for over 4 months (Santoro et al., 2015a). Three different cathodes based on activated carbon (AC), iron-aminoantipyrine (Fe-AAPyr) and bilirubin oxidase (BOx) enzymes were used. All the cathodes tested had the same current collector that was metallic stainless steel mesh (McMaster, USA).

AC-based cathode was prepared by mixing 70%wt high surface area AC (Norit SX Ultra, Sigma Aldrich), 10%wt carbon black (CB, Alfa Aesar) and 20%wt PTFE (60% solution, Sigma Aldrich) for 5 min in a coffee grinder. The carbon black was added to enhance the composite electrode conductivity. After mixing, the composite material was pressed at 2 mT into a pellet die for 5 min (Santoro et al., 2014). The composite loading was 35±5 mg cm^{-2}, the geometric area was 2.25 cm^2 and this value was used for the power normalization. The cathode has not been heated as previously shown (Santoro et al., 2014). The volume used for power normalization refers to the chamber volume of 125 mL.

156 The same procedure was followed to prepare Fe-AAPyr based cathode except that Fe-
157 AAPyr was added into the mixture and mixed vigorously, before pressing at 2 mT. The
158 preparation of Fe-AAPyr has been previously described (Santoro et al., 2015b). The Fe-
159 AAPyr loading was 1.5 ± 0.1 mg cm^{-2}. Synthetic approach for preparation of Fe-AAPyr
160 was based on Sacrificial Support Method developed at University of New Mexico. (Serov
161 et al., 2014a, 2014b)
162 The preparation of BOx cathode instead was based on AC (70%wt), 10%wt CB and
163 20%wt PTFE ground for 5 min and then pressed at 2 mT for 5 min. After that,
164 isopropanol (40 μL cm^{-2}) was added on the top to create a hydrophilic/hydrophobic
165 gradient. A multi-walled nanotube paper (MWNTP, Buckeye Composite) was then fused
166 together on the top using pressure 0.25 mT for 5 min). At last, 10 mg of BOx (Amano
167 Enzyme, USA) dissolved in 50 mM PBS solution was then drop-casted onto the MWNTP
168 surface. The cathodes were kept at 4°C over night for enzyme immobilization. Before the
169 utilization, the liquid was dried and then the cathode was screwed on the lateral hole of
170 the bottle (Santoro et al., 2013).
171 The additional cathode for the supercapacitor was carbon brush (Millirose, USA) of
172 diameter 2 cm and projected area of 4 cm^2 that was coated with a 95%wt AC- 5%wt
173 Nafion layer (0.3 g total). The carbon brush was immersed into a solution based on
174 Nafion (0.5% alcoholic solution Dupont, 1.0 mL), AC (100 mg) and water-isopropanol
175 solution (1 mL) and then was dried in ambient atmosphere over night. The addition of
176 AC allowed the increase in surface area of the carbon brush and consequently in the
177 capacitance of the overall additional cathode brush. The additional cathode was
178 completely immersed into the electrolyte and short-circuited with the MFC cathode.

2.3 Electrochemical measurements

Electrochemical measurements have been done using a potentiostat (SP-50, Bio-Logic, France). Electrochemical tests consisted in the repetition of a sequence of the following steps: rest (OCV) – galvanostatic (GLV) discharge at different currents (i_{pulse}, A) from 1 mA up to 45 mA) over 10 ms, 2 s or complete discharge down to 0V cell voltage. The use of the reference electrode permitted to simultaneously monitor the MFC anode and cathode (eventually short circuited with the AdC cathode) potentials as well as the cell voltage during the sequence repetition. The analysis of the GLV discharge data is detailed in the ESI section

3. Results and discussion

3.1 Supercapacitive Microbial Fuel Cell

PLEASE INSERT HERE FIGURE 1

In rest conditions, the cell voltage ($V_{max, OC}$) of an MFC is determined by the equilibrium potentials of the half-reactions taking place at the electrodes. The anaerobic anode equilibrium potential of acetate oxidation at pH=7 is equal to ~-500 mV vs Ag/AgCl. The theoretical potential for the oxygen reduction reaction at pH=7 is ~620 mV vs Ag/AgCl (Erable et al., 2012). The anaerobic (bio-anode) and aerobic (cathode) environments of

202 the MFC polarize the carbon electrodes towards values that are more negative and
203 positive than the typical equilibrium potential (near 0 mV vs Ag/AgCl (Béguin et al.,
204 2014)) exhibited by metal and catalyst-free carbons in the de-aerated electrolytes (e.g.
205 supercapacitors electrolytes). The electrode processes cause the formation of
206 electrochemical double layers at the MFC electrode/electrolyte interfaces (Conway,
207 1999).
208 The excess of negative and positive charges, at the polarized anode and cathode surfaces
209 respectively, is balanced by positive and negative counter ions coming from the ionic
210 species dissolved in the solution. Electrolyte ions migrate to oppositely charged
211 electrodes forming an electrochemical double layer at each high-surface area
212 carbonaceous electrode of the MFC. The MFC is electrostatically storing charge at
213 $V_{max,OC}$, hence it is storing energy like in the case of an EDLC. The MFC anode and
214 cathode can be then discharged by a rapid electrostatic process. Their surface charges are
215 neutralized and ions are released in the bulk wastewater solution. The energy that was
216 electrostatically stored can thus be delivered by high and short galvanostatic discharge
217 pulses (GLV) and high power output is achieved. Subsequent rest, i.e. setting the MFC in
218 OC without any external load applied, restores the electrode equilibrium potentials. The
219 carbon electrodes are polarized again, the double-layers at each electrode are re-
220 established, and the internal EDLC is recharged. Under these conditions, the system
221 operates a self-powered supercapacitor (Fig. 1.a and Fig. 1.b).
222 Fig. 1.c reports the cell voltage trend of a MFC under a rest (OC) - galvanostatic
223 discharge pulse (GLV) - OC sequence. Fig. 1.c also highlights the parameters that were
224 used for the evaluation of the system performance (see Supplemental Information).

225

226 **PLEASE INSERT HERE FIGURE 2**

227

228 For the first time, this concept was proven by the data reported in Figure 2 that shows the
229 MFCs cell voltage and electrode potential profiles under the sequence test reported in
230 Fig. 1.c, by 2 s (t_{pulse}) discharge pulse at 3 mA (i_{pulse}). The MFCs investigated had
231 different cathodes described before as AC, Fe-AAPyr and BOx and the cells are labeled
232 with the cathode acronyms. The AC, Fe-AAPyr and BOx MFCs features V_{max}, OC of 590
233 mV, 650 mV and 790 mV, respectively. This trend follows the equilibrium cathode
234 potentials of 105, 175 and 315 mV vs Ag/AgCl for AC, Fe-AAPyr and BOx cathodes.
235 Higher cathode potentials of BOx compared to other catalysts have been previously
236 shown (Mano et al., 2003). In all the investigated MFCs the equilibrium anode potential
237 was ≈-500 mV vs Ag/AgCl which is close to the theoretical value.
238 The pulse caused the decrease of V_{max}, OC by ohmic (ΔV_{ohmic}) and capacitive
239 ($\Delta V_{capacitive}$) contributions (Fig. 1.c). The ΔV_{ohmic} cell voltage losses were in the range of
240 311 mV to 383 mV (Fig. 2 a,c,e) which were due to ESRs of 105-130 Ω (Table S1,
241 calculation in SI). Monitoring the MFC electrode potentials during the pulse permitted to
242 identify the cathode as the main contributor of ΔV_{ohmic} and, hence, of ESR for all the
243 MFCs (Fig. 2.b,d,f). Cathode overpotentials at i_{pulse} equal to 3 mA were 299 mV for BOx,
244 followed by Fe-AAPyr with 339 mV and AC with 344 mV and accounted for over 90%
245 of the total MFC ΔV_{ohmic} and ESR. The high electrode thickness (≈1 mm) that is required
246 to avoid wastewater leakage through the breathing cathode could be one of the
247 parameters that determine the high cathode impedances (in the order of 100 Ω, as

248 evaluated by dividing the cathode overpotential by i_{pulse}). The lowest ohmic losses of
249 BOx cathode can be related to the utilization of CNT in the electrode preparation. CNT
250 enhanced electronic conductivity compared to AC-based electrodes. The anodes based on
251 carbon brush colonized by electro-active bacteria featured very low overpotentials within
252 few mV (accounted for less than 10% of the total MFC ΔV_{ohmic} and ESR). This suggests
253 that using high surface area and high conductivity carbon brush contributed to very low
254 anode impedance that varied in a small range of 4-13 Ω.
255 For all the MFCs, the $\Delta V_{capacitive}$ cell voltage loss of the different MFCs was negligible
256 and similar, indicating comparable cell capacitance (C) response. The values of C
257 estimated by the cell voltage slope (s) (Conway, 1999) were between 80 and 100 mF
258 (Table S1, calculation in SI). The electrode profile analyses indicated that anode and
259 cathode almost equally contribute to C with electrode capacitances of ca. 200 mF.
260 Capacitance (C), equivalent series resistance (ESR), and maximum cell voltage under
261 operation (V_{max}), which in turn depends on ESR (see SI), determine the practical
262 maximum energy (E_{max}) and power (P_{max}) and the charge/discharge time constant (τ) of
263 the supercapacitor. Indeed, these parameters are related by the following equations:

264 $$E_{max} = ½\ C \times V_{max}^2 \quad (1)$$

265 $$P_{max} = i_{pulse} \times V_{max} \quad (2)$$

266 $$\tau = ESR \times C. \quad (3)$$

267 C and ESR were used to estimate τ (Table S1) which was in the order of 10 s, thus
268 demonstrating the fast rate capability of the supercapacitive system. Table S1 reports the
269 practical values of E_{max} and P_{max}, and of the useful energy delivered during the pulse
270 (E_{pulse}) and average pulse power (P_{pulse}) evaluated by the GLV curves at 3 mA reported on

Fig. 2. These values were calculated by taking into account that the highest feasible cell voltage (V_{max}) is the voltage of the charged cell in open circuit conditions ($V_{max,\ OC}$) decreased by ΔV_{ohmic} after the pulse (see Figure 1.c), which in turn depends on i_{pulse} (eqs. SI9 and SI10). The energy and power values increase in the order AC < Fe-AAPyr < BOx, thus following the MFC voltage trend.

PLEASE INSERT HERE FIGURE 3

On the basis of ΔV_{ohmic} and ESR that were evaluated by the test reported in Fig. 2, we calculated the P_{max} that can be delivered by the three MFCs at different i_{pulse} as described in the Data Analysis Section of the SI, and the data are reported in Fig. 3. The Figure reports P_{max} values that are 3-5 times higher compared to the highest values obtained during conventional MFC operations that with the same configuration were equal to 2 Wm^{-2} (BOx) (Santoro et al., 2013), 1.67 Wm^{-2} (Fe-AAPyr) (Santoro et al., 2015b) and 1.17 Wm^{-2} (AC) (Santoro et al., 2015b) referred to the geometric area of the cathode, the limiting electrode.

Fig. 3 even indicates that the MFCs can deliver pulse currents up to 4 mA (AC and Fe-AAPyr) and 5 mA (BOx). We calculated that the highest P_{pulse} of 1.47 mW (6.53 Wm^{-2}, 11.76 Wm^{-3}) can be delivered by the BOx MFC at 3.7 mA, followed by Fe-AAPyr-MFC (0.90 mW (4 Wm^{-2}, 7.2 Wm^{-3}) at 2.7 mA) and AC (0.67 mW (2.98 Wm^{-2}, 5.36 Wm^{-3}) at 2.2 mA).

292 Data in Table S1 and Fig. 3 demonstrate that the utilization of cathodes with high
293 working potentials is a reasonable option to increase the electric work and the power
294 output of the designated current pulse.
295
296 **3.2 MFC-AdC Response**
297 ESR, C, i_{pulse} and t_{pulse} are the key parameters to be optimized in order to achieve high
298 maximum energy (E_{max}) and power (P_{max}) and, more importantly, high practical values of
299 energy (E_{pulse}) and power (P_{pulse}) delivered during the pulses. The practical values of E_{max}
300 and P_{max} depend on the highest feasible cell voltage (V_{max}), namely the voltage of the
301 charged cell in open circuit conditions ($V_{max, OCV}$) decreased by ΔV_{ohmic} after the pulse,
302 which in turn depends on ESR and i_{pulse} (see SI). ESR has to be minimized in order to
303 increase power output. The performance of the MFCs reported above was mainly
304 affected by the cathode ohmic losses. In order to overcome cathode limitation, an
305 additional cathode (denoted as AdC) was short-circuited with the MFC cathode,
306 embedded into the same electrolyte, and used as the positive electrode of the internal
307 supercapacitor (Fig. 1.b). The AdC was a carbon brush coated with activated carbon (AC)
308 to increase its surface area and electrode capacitance. The brush was used for its low
309 electrode resistance demonstrated in the previous section 3.1.
310 The AdC was short-circuited with the MFC cathode and it was brought to the high
311 potential value of the latter. This caused the formation of an electric double-layer at the
312 short-circuited brush/wastewater interface and the internal, positive charge of the AdC
313 (Fig. 1.b). Coupling the AdC with the MFC anode provides an internal, self-powered
314 EDLC that can be rapidly discharged by an electrostatic process to give high power

315 output. According to the Kirchhoff law, the highest current will flow through the lowest
316 resistance branches of the circuit that models our system, i.e. the MFC anode and AdC
317 electrode resistances and the electrolyte resistance. The MFC cathode is then excluded
318 with positive effect on ESR and power output.
319 The MFC-AdC cells with AC, Fe-AAPyr and BOx cathodes short-circuited with the AdC
320 are labeled with AC-AdC, Fe-AAPyr-AdC, and BOx-AdC. Fig. 3 shows the cell voltage
321 and electrode potential profiles under 2 s discharge pulse at 3 mA. The MFC-AdC
322 performances are summarized in Table S1.
323 Fig. 2 a, c, e demonstrate that the use of the AdC with i_{pulse} equal to 3 mA dramatically
324 decreases ΔV_{ohmic} down to 66 mV, 50 mV and 56 mV with AC, Fe-AAPyr and BOx
325 cathodes, without modifying the corresponding $V_{max, OC}$. The MFC-AdC ESRs evaluated
326 by ΔV_{ohmic} are 6-8 times lower than MFCs' and reduced to 16-22 Ω. Fig. 2b, d, f evinces
327 that this result is due to the very low potential losses of the AdC-short circuited cathodes,
328 in turn related to their low impedances of ≈13 Ω. Given that the cell capacitance did not
329 significantly change (except for the cell with Fe-AAPyr-AdC which exhibited 60 mF),
330 the time response τ was substantially lowered to 2 s.
331 Table S1 demonstrates that the decreases of ΔV_{ohmic} had the main effect on V_{max} and on
332 energy and power values which substantially increased. The highest performance was
333 achieved with the BOx-AdC cell which at 3 mA featured a practical operation voltage of
334 734 mV and P_{pulse} of 2 mW (t_{pulse} = 2 s). These are extremely high values that have never
335 been reported before for microbial fuel cells.
336
337 **PLEASE INSERT HERE FIGURE 4**

The MFC-AdC cells were also tested at different pulse currents and the voltage profiles analyzed to extract the P_{max} vs I_{pulse} plots reported in Fig. 4 (see SI). The significant decrease in ESR allow to achieve pulse current up to 45-50 mA that were roughly 10 times higher than the 4-5 mA possible with MFC. P_{max} was 19 mW (84.4 Wm^{-2}, 152 Wm^{-3}) with BOx cathode, 14 mW (62.2 Wm^{-2}, 112 Wm^{-3}) with Fe-AAPyr and 6 mW (26.7 Wm^{-2}, 49 Wm^{-3}) with AC cathode. These values are roughly one order of magnitude higher than those achieved without AdC (Fig. 3), thus indicating the successful utilization of the AdC.

PLEASE INSERT HERE FIGURE 5

Fig. 5 shows the MFC-AdC average pulse power P_{pulse} delivered at different currents over 10 ms and 2s pulses. Even under such test, the BOx-AdC cell outperformed the other MFC-AdCs having 10 ms power output of 12 mW, followed by 9.5 mW of Fe-AAPyr-AdC and 4 mW of AC-AdC (Fig. 5.a). As it expected, the power decreases at pulse length of 2 s and the highest P_{pulse} was 5 mW for BOx-AdC, followed by 3 mW for Fe-AAPyr-AdC and 2 mW for AC-AdC (Fig. 5.b).

3.3 Supercapacitive recharging time and durability experiments

PLEASE INSERT HERE FIGURE 6

Despite the higher OCP of the BOx, it has been shown previously that enzymes are not durable for long period of time mainly due to denaturation or deactivation (Santoro et al. 2013). Moreover, currently, the cost of BOx is very high limiting practical utilization for wastewater treatment purposes. At the contrary, Fe-AAPyr is a reliable catalyst for oxygen reduction reaction at neutral pH due to its stability and low cost aiming to be a good candidate for large-scale application (Santoro et al. 2015a). Consequently, the recharging time and durability tests have been carried out considering the MFC-AdC with Fe-AAPyr cathode for possible real and long terms application.

Fig. 6.a shows the voltage and electrode potential profiles of the Fe-AAPyr-AdC cell under an OC-GLV-OC sequence with 2s-pulses at 6 mA and 20 s rest. The rest of 20 s was enough to restore the equilibrium electrode potentials and "recharge" the cell at the $V_{max,\ OC}$ voltage (Fig. 6.b). Each cycle overlapped indicating the reversibility of the process. This underlines that the self-recharge of the internal EDLC is reversible and fast and can take place in the order of seconds.

The cycling stability of the Fe-AAPyr-AdC was proved over 1000 OC-GLV-OC steps which were performed by 10 ms-pulses at 10 mA followed by 10s rest. The first four (Fig. S1c) and last four (Fig. S1d) cycles are also reported. The cell voltage as well as the anodic and cathodic potentials during the initial and final cycles had very similar trend thus indicating that high current regimes (10 mA) do not affect the performances of the cell. Equilibria anode and cathode potentials are recovered in few seconds and this permits a stable, long-time operation.

3.4 Significance of the Supercapacitive Microbial Fuel Cell

In this first proof of concept, we demonstrate that current/power output is comparable with MFC/external supercapacitor systems' with the advantage of much shorter recharging time: sec/min instead of hours. This permits to increase power output frequency that is an appealing feature for real applications where devices need to be frequently powered. Notably, the AdC size can be independently sized which makes it possible to de-couple energy and power and to address target application requirements, from sensor to external pump powering for self-sustainable systems. At last, the proposed concept is sustainable in terms of materials, processes and energy cost. Further works will be addressed to cell design and materials optimization for system scaling up.

4. Conclusions

To the best of our knowledge, for the first time a supercapacitive system with MFC anode and cathode used as negative and positive electrodes of a self-rechargeable, internal supercapacitor is demonstrated. The use of high voltage operation cathodes and the additional capacitive cathode electrode permitted to achieve the exceptionally high power of 19 mW under pulse currents as high as 45 mA. The power normalized to the geometric cathode area results 84 W m^{-2}. This is the highest performance ever achieved by an MFC system. With respect to MFC/external supercapacitor coupling, MFC-AdC is a more efficient, simple and cheap way of harvesting energy from the MFC system and does not require any additional electronics management.

Acknowledgements

This project was funded by the Electrochemical Society and Bill & Melinda Gates Foundation under initiative: “Applying Electrochemistry to Complex Global Challenges”. FS and CA acknowledge financial support by Alma Mater Studiorum - Università di Bologna (Researcher Mobility Program).

References

Agnès, C., Holzinger, M., Le Goff, A., Reuillard, B., Elouarzaki, K., Tingry, S., Cosnier S., 2014. Energy Environ. Sci. 7, 1884-1888

Antolini, E., 2015. Biosens. Bioelectron. 69, 54-70.

Béguin, F., Presser, V., Balducci, A., Frackowiak, E., 2014. Carbons and electrolytes for advanced supercapacitors. Adv. Mater. 26(14), 2219-2251

Conway, B.E., 199. Electrochemical Supercapacitors: Scientific Fundamentals and Technological Applications, Springer.

Deeke, A. Sleutels, T.H.J.A., Hamelers, HV.M., Buisman, C.J.N., 2012. Environ. Sci. Technol. 46(6), 3554–3560

Dewan, A., Ay, S.U., Karim, M.N., Beyenal, H., 2014. J. Power Sources, 245, 129-143

Di Lorenzo, M., Thomson, A.R., Schneider, K., Cameron, P.J., Ieropoulos, I., 2014. Biosens. Bioelectron. 62, 182-188

Donovan, C., Dewan, A., Peng, H., Heo, D., Beyenal, H., 2011. J. Power Sources, 196(3), 1171-1177

429 Donovan, C., Dewan, A., Heo, D., Lewandowski Z., Beyenal, H., 2013. J. Power
430 Sources, 233, 79−85.
431 Erable, B., Féron, D., Bergel, A., 2012. ChemSusChem 5(6), 975-987
432 Ewing, T., Ha, P.T., Babauta, J.T., Tang, N.T., Heo, D., Beyenal, H., 2014. J. Power
433 Sources 272, 311-319.
434 Feng, C., Lv, Z., Yang, X., Wei, C. Anode modification with capacitive materials for a
435 microbial fuel cell: an increase in transient power or stationary power, PCCP, 16
436 (2014) 10464-10472
437 Guerrini, E., Cristiani, P., Grattieri, M., Santoro, C., Li, B., Trasatti, S., 2014. J.
438 Electrochem. Soc. 161 (3), H62-H67
439 Higgins, S.R., Lau, C., Atanassov, P., Minteer, S.D., Cooney, M.J., 2011. ACS Catal., 1
440 (9), 994–997
441 Ieropoulos, I., Melhuish, C., Greenman J., Horsfield, I., 2005. Journal of Advanced
442 Robotic Systems, 2(4), 295-300
443 Ieropoulos, I., Greenman, J., Melhuish C., Horsfield, I., 2010. EcoBot-III-A Robot with
444 Guts. ALIFE, 733-740.
445 Ieropoulos, I.A., Greenman, J., Melhuish, C., Horsfield, I., 2012. ChemSusChem
446 5(6),1020-1026
447 Ieropoulos, I.A., Ledezma, P., Stinchcombe, A., Papaharalabos, G., Melhuish, C.,
448 Greenman, J., 2013. Phys. Chem. Chem. Phys. 15(37), 15312-15316
449 Ishii, S., Suzuki, S., Norden-Krichmar, T.M., Phan, T., Wanger, G., Nealson, K.H.,
450 Sekiguchi, Y., Gorby Y.A., Bretschger, O., 2014. ISME J., 8(5), 963-978

451 Jang, J.K., Kan, J., Bretschger, O., Gorby, Y.A., Hsu, L., Kim, B.H., Nealson, K.H.,
452 2013. J. Microbiol. Biotechnol. 23(12), 1765-1773.
453 Ledezma, P., Stinchcombe, A., Greenman J., Ieropoulos, I., 2013. Phys. Chem. Chem.
454 Phys. 15, 2278-2281
455 Liu, X.-W., Li, W.-W., Yu, H.-Q., 2014. Chem. Soc. Rev., 43, 7718—7745
456 Logan B.E., Rabaey, K., 2012. Science 337, 686-690
457 Lv, Z., Xie, D., Yue, X., Feng C., Wei, C., 2012. J. Power Sources 210, 26–31
458 Mano, N., Fernandez, J.L., Kim, Y., Shin, W., Bard, A.J., Heller, A., 2003. J. Am. Chem.
459 Soc. 125(50), 15290–15291
460 Pankratov, D., Falkman, P., Blum Z., Shleev, S., 2014a. Energy Environ. Sci., 7, 989-
461 993.
462 Pankratov, D., Blum, Z., Suyatin, D.B., Popov V.O., Shleev, S., 2014b.
463 ChemElectroChem 1(2), 343-346.
464 Papaharalabos, G., Greenman, J., Melhuish, C., Santoro, C., Cristiani, P., Li, B.,
465 Ieropoulos, I., 2013. Int. J. Hydrogen Energy 38(26), 11552-11558
466 Papaharalabos, G., Greenman, J., Stinchcombe, A., Horsfield, I., Melhuish, C.,
467 Ieropoulos, I., 2014. J. Power Sources, 272, 34-38
468 Park, J.-D., Ren, Z.J., 2012. J. Power Sources 208, 322−327.
469 Pocaznoi, D., Calmet, A., Etcheverry, L., Erable, B., Bergel, A., 2012. Energy Environ.
470 Sci., 5, 9645-9652
471 Rinaldi, A., Mecheri, B., Garavaglia, V., Licoccia, S., Di Nardo, P., Traversa, E., 2008.
472 Energy Environ. Sci., 1, 417-429

473 Santoro, C., Babanova, S., Atanassov, P., Li, B., Ieropoulos, I., Cristiani, P., 2013. J.
474 Electrochem. Soc. 160(10), H720-H726
475 Santoro, C., Artyushkova, K., Babanova, B., Atanassov, P., Ieropoulos, I., Grattieri, M.,
476 Cristiani, P., Trasatti, S., Li, B., Schuler, A.J., 2014. Biores. Technol. 163, 54-63
477 Santoro, C., Serov, A., Narvaez Villarrubia, C.W., Stariha, S., Babanova, S., Schuler, A.,
478 Artyushkova, K., Atanassov, P., 2015a. ChemSusChem 8(5), 828-834
479 Santoro, C., Serov, A., Narvaez Villarrubia, C.W., Stariha, S., Babanova, S.,
480 Artyushkova, K., Schuler, A., Atanassov, P., 2015b. Sci. Rep. In press.
481 Schaetzle, O., Barrière F., Schröder, U., 2009. Energy Environ. Sci. 2, 96-99.
482 Serov, A., Artyushkova, K., Atanassov, P., 2014a. Adv. Energy Mater., 4, 1301735 doi:
483 10.1002/aenm.201301735.
484 Serov, A., Tylus, U., Artyushkova, K., Mukerjee, S., Atanassov, P., 2014b. Appl. Catal.,
485 B, 150, 179-186
486 Soukharev, V., Mano, N., Heller, A., 2004. J. Am. Chem. Soc. 126(27), 8368–8369
487 Wang, H., Park, J., Ren, Z.J., 2015. Environ. Sci. Technol. 49, 3267-3277
488 Watson, V.J., Delgado, C.N., Logan, B.E., 2013. Environ. Sci. Technol., 47(12),
489 6704−6710
490 Wei, J., Liang, P., Huang, X., 2011. Biores. Technol. 102, 9335–9344

Figures Content

Figure 1. Microbial Fuel Cell configuration with anode and cathode of the MFC used as EDLC electrodes. Red and blue circles indicate cations and anions, respectively (a). MFC-AdC configuration with short circuited AdC-cathode and anode of the MFC used as EDLC electrodes (b). Current/Cell Voltage trends during the OC – GLV- OC sequence used for the electrochemical test. The labels indicate the parameters used for the evaluations of the system performance (c).

Figure 2. Cell voltage (a,c,e) and electrode potential (b,d,f) profiles of MFC and MFC-AdC cells with AC (a,b), Fe-AAPyr (c,d) and BOx (e,f) cathodes under 5s rest and 2 s pulses at 3 mA.

Figure 3. Calculated P_{max} vs. i_{pulse} plots of the MFCs assembled with AC, BOx and Fe-AAPyr cathodes.

Figure 4. P_{max} vs. i_{pulse} plots of the three MFCs having the additional cathode calculated at different pulse currents.

Figure 5. P_{pulse} vs. i_{pulse} plots for MFC-AdC cells for pulse time of 10 ms (a) and 2 s (b).

Figure 6. Cell voltage (a) and anode and cathode potentials (b) profile of a Fe-AAPyr-AdC cell under an OC-GLV-OC sequence with 2s-pulses at 6 mA and 20 s rest.

Figure 1

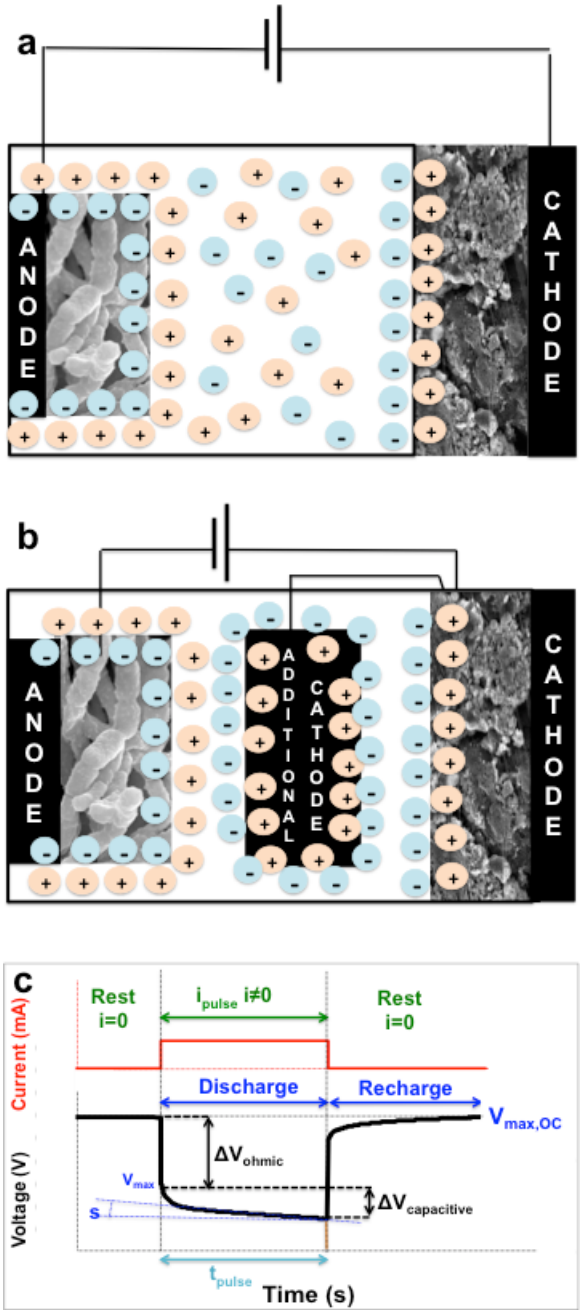
a
ANODE
CATHODE
b
ANODE
ADDITIONAL CATHODE
CATHODE
c
Rest i=0
i_{pulse} i≠0
Rest i=0
Discharge
Recharge
$V_{max,OC}$
ΔV_{ohmic}
V_{max}
$\Delta V_{capacitive}$
s
t_{pulse}
Current (mA)
Voltage (V)
Time (s)

Figure 2

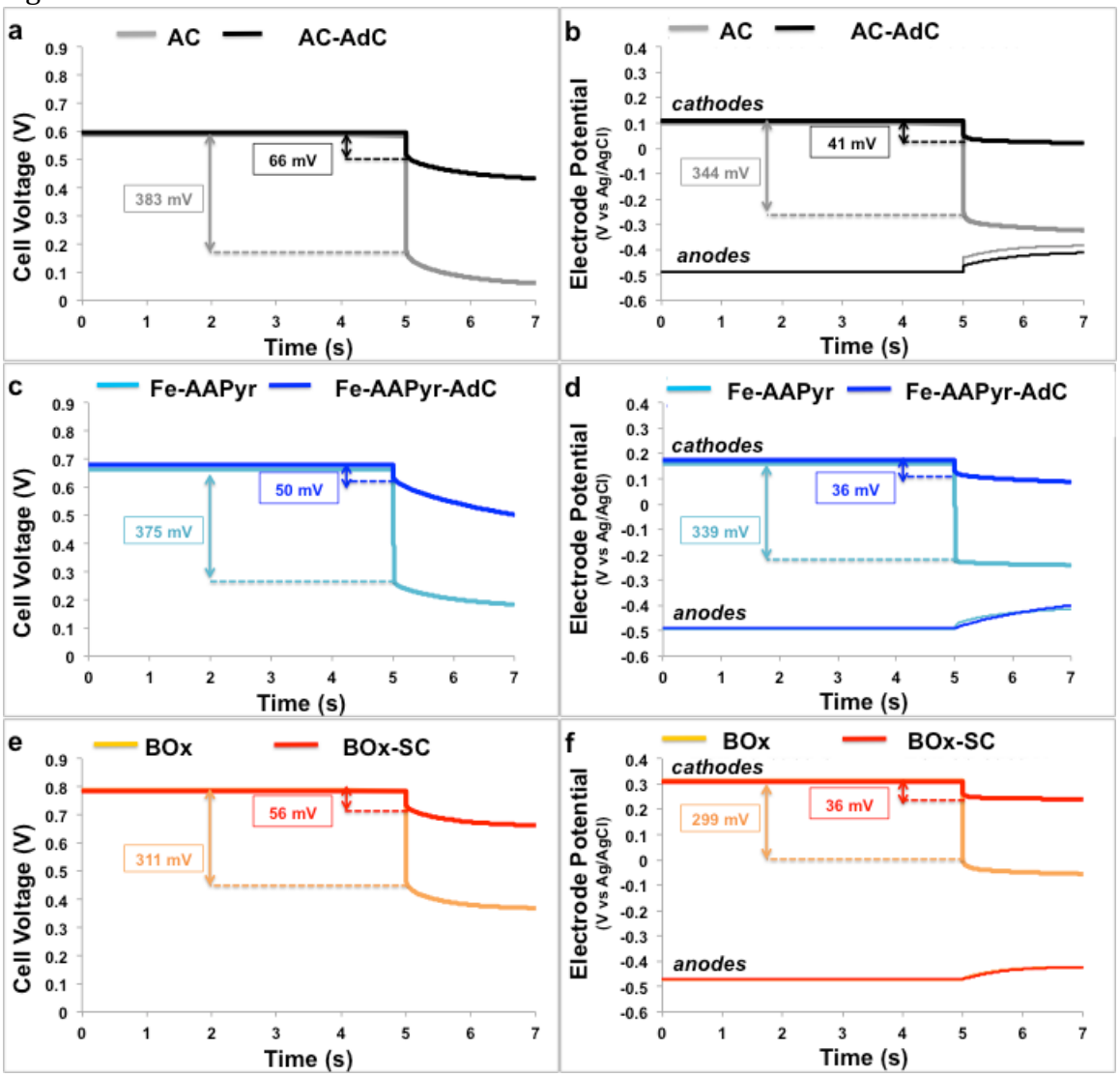
a
AC
AC-AdC
Cell Voltage (V)
Time (s)
66 mV
383 mV
b
AC
AC-AdC
Electrode Potential
(V vs Ag/AgCl)
cathodes
anodes
41 mV
344 mV
Time (s)
c
Fe-AAPyr
Fe-AAPyr-AdC
Cell Voltage (V)
Time (s)
50 mV
375 mV
d
Fe-AAPyr
Fe-AAPyr-AdC
Electrode Potential
(V vs Ag/AgCl)
cathodes
anodes
36 mV
339 mV
Time (s)
e
BOx
BOx-SC
Cell Voltage (V)
Time (s)
56 mV
311 mV
f
BOx
BOx-SC
Electrode Potential
(V vs Ag/AgCl)
cathodes
anodes
36 mV
299 mV
Time (s)

Figure 3

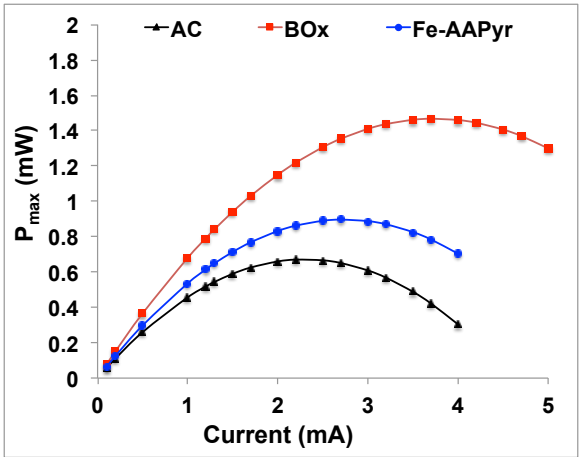

Figure 4

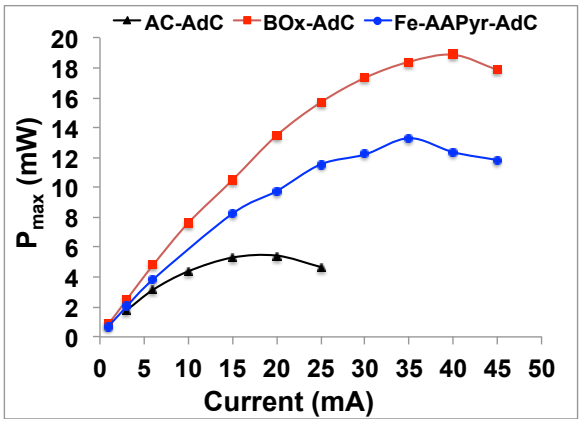

Figure 5

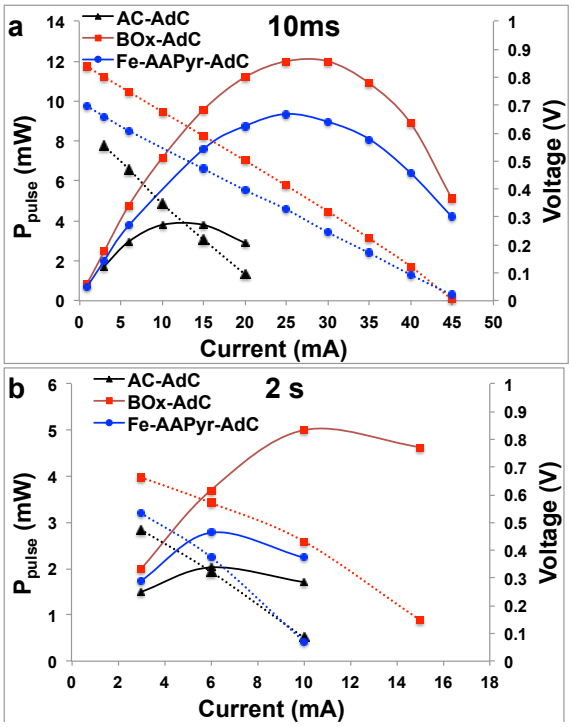
a
10ms
AC-AdC
BOx-AdC
Fe-AAPyr-AdC
P pulse (mW)
Voltage (V)
Current (mA)
b
2 s
AC-AdC
BOx-AdC
Fe-AAPyr-AdC
P pulse (mW)
Voltage (V)
Current (mA)

Figure 6

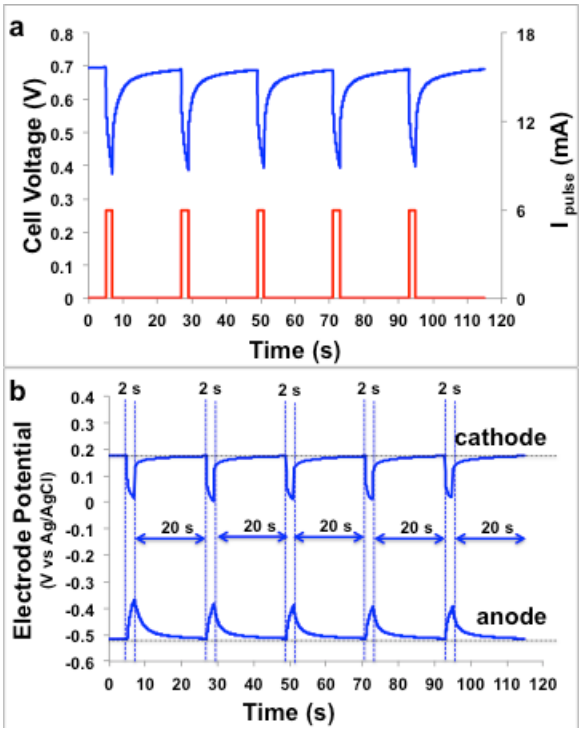
a
Cell Voltage (V)
0.8
0.7
0.6
0.5
0.4
0.3
0.2
0.1
0
18
12
6
0
I pulse (mA)
0 10 20 30 40 50 60 70 80 90 100 110 120
Time (s)
b
Electrode Potential
(V vs Ag/AgCl)
2 s
2 s
2 s
2 s
2 s
cathode
20 s
20 s
20 s
20 s
20 s
anode
0.4
0.3
0.2
0.1
0
-0.1
-0.2
-0.3
-0.4
-0.5
-0.6
0 10 20 30 40 50 60 70 80 90 100 110 120
Time (s)